Phase transition in hydrogen-bonded 1-adamantane-methanol

Bacem Ben Hassine[1,3], Philippe Negrier[1], María Barrio[2], Denise Mondieig[1], Stéphane Massip[4] and Josep Ll. Tamarit[2,*]

[1]Université de Bordeaux, LOMA, UMR 5798, F-33400 Talence, France, CNRS, LOMA, UMR 5798, F-33400 Talence, France.

[2]Grup de Caracterització de Materials, Department de Física i Enginyeria Nuclear, ETSEIB, Diagonal 647, Universitat Politècnica de Catalunya, 08028 Barcelona, Catalonia (Spain)

[3]Laboratoire des Matériaux Céramiques Composites et Polymères, LaMaCoP, Département Physique, Faculté des sciences de Sfax, 3000 Sfax (Tunisie)

[4]Institut Européen Chimie & Biologie, Université de Bordeaux, CNRS UMS 3033, INSERM US001, F-33607 Pessac, France

[*] josep.lluis.tamarit@upc.edu

Abstract

The polymorphism of 1-adamantane-methanol $C_{11}H_{18}O$ has been investigated by differential thermal analysis and single-crystal and powder X-ray diffraction. Below the melting temperature (389.5 ± 0.4 K), this compound exhibits an orthorhombic phase (Phase I, Pnnm, Z=12, Z'=1.5). The melting enthalpy was determined to be 20.5 ± 0.4 kJ mol^{-1}, i.e., with an entropy change of (6.34 ± 0.13)R, which is much higher than the quoted value from Timmermans for the melting orientationally disordered phases (2.5R), thus supporting the orientationelly ordered character of phase I. This orthorhombic phase I exhibits a statistical disorder of the hydrogen atom related to the oxygen atom, due to the position of one independent molecule on the mirror. At ca. 272 K, phase I transforms continuously through an order-disorder transition to a low-temperature monoclinic phase II ($P2_1/n$, Z=12, Z'=3). The monoclinic and orthorhombic phases are related by a group-subgroup relationship, which perfectly agrees with the continuous character of the II to I transition. Moreover, by a convenient choice of an order parameter related to the continuous tilt of the c-axis, the critical exponent for this transition is found to be close to the theoretical prediction of 3D-Ising model (with a critical exponent is of ca. 0.27).

1. Introduction

Diamondoids are organic compounds with unique structures and properties. This family of compounds is one of the best candidates for self-assembled process in a large number of applications as chemical processes, many applications in nanotechnology as well as in biological and pharmaceutical domains. [1-6]

Diamondoids have recently acquired great interest owing to their important role in industrial chemicals, in particular, for building up organic crystals with large cavities and useful physical and chemical properties. [7-12]

The simplest member of the diamondoid group is the adamantane molecule, $C_{10}H_{16}$, which is a rigid molecule with point group symmetry T_d formed by 10 carbon atoms arranged as a single diamond cage surrounded by 16 hydrogen atoms. [13]

Recently, adamantane derivative molecules have been used for gel systems by mixing 1-adamantanecarboxilic acid and 1-adamantylamine owing to the hydrogen bonding between carboxylic acid and amine groups. [14] This system is seen as a colloidal system with nanometer particles (formed by the aforementioned molecules strongly linked) interacting through van der Waals forces.

The replacement of one or more hydrogen atoms in the molecule of adamantane by a substituent X (X= OH, F, Cl, I, etc.) modifies the symmetry of the molecule, its polarity, intermolecular interactions and steric effects, in particular in solid phases. There are two positions on the adamantane cage where single substitution can occur: the 1-X position, with a highly reactive tertiary carbon, where the molecule retains a C_{3v} point-group symmetry, and the 2-X position, with a secondary less reactive carbon atom, which gives rise to molecules with C_{2v} symmetry. Although the number of studies concerning 2-X-adamantane derivatives is less extensive, detailed polymorphic studies have also been reported. [15-22]

The phase behavior of the 1-X adamantane compounds varies according to the substituent. Most of these derivatives show up an orientationally disordered (plastic) phase prior to fusion, for example, 1-chloroadamantane, 1-bromoadamantane and 1-cyanoadamantane. However, in the case of 1-iodoadamantane, the high-temperature phase is not orientationally disordered. [23-26]

These compounds also may have one or several solid-solid transitions. For example, 1-chloroadamantane and 1-bromoadamantane exhibit one and two solid-solid phase transitions, respectively. [27] These adamantane derivatives show a rich polymorphic behavior that has largely been studied. [28-36]

The physical and chemical properties, even for the simple adamantane derivatives have not been studied for some of them in which the substitution concerns more than a halogen atom. Among these adamantane derivatives, 1-CH_2OH-adamantane (1-adamantane-methanol, $C_{11}H_{18}O$) is one for which no studies have been conducted till present. In this paper, the polymorphism of this compound as well as the mechanisms of solid-solid transition~~s~~ has been undertaken by means of a combination of several experimental techniques, thermal analysis and powder and single-crystal X-ray diffraction. The structures for the different phases have been determined and compared for the first time.

2. Experimental details

2.1. Materials. 1-adamantane-methanol ($C_{11}H_{18}O$) was purchased from Sigma Aldrich with purity of 99%. It was used after further purification by sublimation under partial vacuum at 323K.

2.2. Differential thermal analysis. The thermal properties of the phase transitions (temperature and enthalpy changes) were determined by a Perkin Elmer DSC-7 instrument. Heating and cooling rates of (2 K.min^{-1} and 10 K.min^{-1}) under a constant nitrogen stream and powder samples with mass between 4 mg and 10 mg were used. A TA-Instruments Q100 system was used with an intracooler system for the low-temperature specific heat measurements through the modulation function. In such a case scanning rates of 1 K.min^{-1} with modulation of ±0.5 K every 60 s were used.

2.3. High-pressure differential thermal analysis. The transitions were studied with home-made high-pressure differential thermal analyzers (HP-DTA) for low- and for high-temperature. [37] These systems enable to cover the temperature range between 200 K and 470 K within a pressure range from normal pressure to 300 MPa. Samples were sealed in cylindrical tin pans by melting the studied substance taking care that no residual air remains. HP-DTA scans were carried out with a heating rate of 2 K.min^{-1}.

2.4. Powder X-ray diffraction measurements. Powder X-ray diffraction data were collected by means of a horizontally mounted INEL cylindrical position-sensitive detector (CPS 120). The detector, used in Debye-Scherrer geometry, is constituted by channels, providing an angular step of 0.029° (2θ) between 4° and 120°. Monochromatic Cu $K_{\alpha 1}$ radiation (λ= 1.5406 Å) was selected with an asymmetric focusing incident-beam curved quartz monochromator. The angular linearity deviation in PSD (position-sensitive detector) was corrected according to the recommended procedure with external calibration and was performed by means of cubic spline fittings. [38] We used the $Na_2Ca_2Al_2F_{14}$ cubic phase mixed with Silver Behenate. The generator power was set to 1.0 kW (40 kV and 25 mA). The peak positions were determined by pseudo-Voigt fittings using the Peakoc application from Diffractinel software. [39] The samples were introduced into 0.5-mm-diameter Lindemann capillaries which rotate along their longitudinal axes during data collection to prevent the effects of the preferred orientations. The system is equipped with a liquid nitrogen 600 series Cryostream Cooler from Oxford Cryosystems with a temperature accuracy of 0.1 K and similar to fluctuations. The X-ray profiles were acquired isothermally after cooling and heating back so that the temperature range was scanned at the intervals of 20 K and less when the transition was approached.

The indexing of the X-ray powder diffraction patterns, structure solutions, Pawley and Rietveld refinements were performed using Materials Studio Program (MS Modeling (Materials Studio), version.5.5.http://www.accelrys.com). [40]

2.5. Single-crystal X-ray diffraction measurements. Several single crystals with different morphologies were picked from the raw product. Due to the twining tendency, a very small single crystal ($0.20 \times 0.12 \times 0.08$ mm^3) was chosen.

The single-crystal X-ray diffraction data were collected at 275 K with an FR-X Rigaku diffractometer with rotating anode Cu-K_α radiation (λ= 1.54187 Å) and a Dectris Pilatus 200 K detector. The unit cell determination and data reduction were performed using the Crystal Clear program suite [41] on the full set of data. The structure was solved by direct methods and refined using Shelx 97 [42] suite of programs in the integrated WinGX system. [43] The positions of the H atoms were deduced from the coordinates of the non-H atoms and confirmed by Fourier synthesis. The non-H atoms were refined with anisotropic temperature parameters.

3. Results and Discussion

The normal pressure thermal analysis of 1-adamantane-methanol was performed from 250K up to the melting. The thermograms (Figure 1-a) have revealed a spread out endothermal effect peaking at ca. 272K associated with a solid-solid transition and an endothermic peak corresponding to the melting, T_{onset}= 389.5±0.4K, with an enthalpy change of 20.5 ± 0.4kJ mol^{-1}. Insert of Figure 1 depicts the specific heat C_p measured by means of modulated calorimetry across the II to I transition. The shape of C_p variation with temperature is clearly reminiscent of a high-order phase transition. Both II to I and I to Liquid temperature transitions increased on increasing pressure (Figure 1-b). The II-I curve is found to be linear ($T = a\,p + T_0$ with a= 0.203 ± 0.004MPa^{-1} and T_0 = 272.27 ± 0.69K), whereas the melting curve is slightly convex, i.e. dT/dp decreases on increasing pressure. In that case, the Anderson-Anderson equation $T = k_1\left(1+\frac{k_2}{k_3}p\right)^{1/k_2}$ [44] was used for describing the experimental points. The best fit (solid line in Figure 1b) was obtained for k_1=388.6 ± 0.4K, k_2 =4.9 ± 0.6 and k_3=1487 ± 68. Within the limit of $p\rightarrow 0$, $\left(\frac{dT}{dp}\right)_{p\rightarrow 0} = \frac{k_1}{k_3} = (0.261 \pm 0.012)$ K.MPa^{-1}. According to the Clausius-Clapeyron equation, $\left(\frac{dT}{dp}\right) = \frac{\Delta v}{\Delta s} = \frac{T\Delta v}{\Delta h}$, where Δs and Δh are the entropy and the enthalpy changes at the transition, a volume change at the melting temperature T of ($\Delta v = v_L - v_s = 13.8 \pm 0.6$) $cm^3.mol^{-1}$ is inferred. Such a volume change provides a relative volume change of $\frac{v_L}{v_s} = 1.09 \pm 0.05$, with v_s=152.7 $cm^3.mol^{-1}$, is the volume of the solid phase obtained at the melting point by extrapolating the values obtained by means of X-ray diffraction, which agrees with the values obtained for many organic systems, for which $\frac{v_L}{v_s} = 1.10 \pm 0.07$. [45] In addition, it must be mentioned that both the volume change at the melting and the slope of the two-phase coexistence curve, $\left(\frac{dT}{dp}\right)$, are close to the volume change at the ordered to orientationally disordered transition for some adamantane derivatives, [46-48] thus reinforcing the orientationally ordered character of phase I for the case here studied. Moreover, the changes of the thermodynamic properties at the melting process do not correlate with the relationships established for orientationally disordered phases. [49-50]

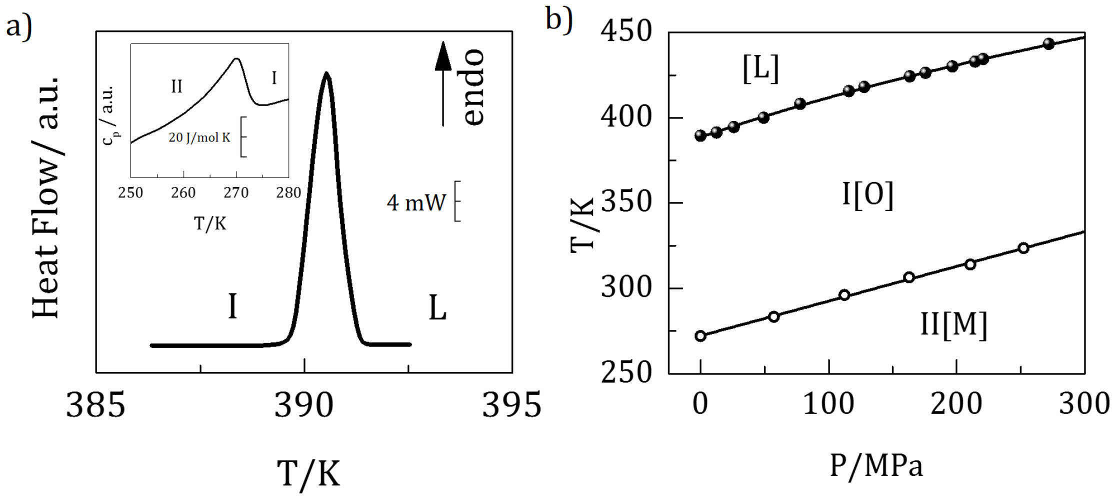

Figure 1: (a) DTA curve of the solid to liquid transition for 1-adamantane-methanol. Insert: Relative specific heat across the solid-solid transition. (b) Solid-solid (empty circles) and melting (full circles) transition temperature curves as a function of pressure. (Some differential analysis curves for a selected pressure values are shown in Supporting Information).

The structure of phase I was solved by means of high-resolution X-ray single-crystal diffraction patterns at 275 K. The lattice of phase I was determined as orthorhombic, space group Pnnm and Z = 12. There are two independent molecules, one molecule in a general position and the other one on the mirror, so Z'=1.5 (see Figures 2-a and 2-c). This orthorhombic phase exhibits a statistical disorder concerning the hydrogen atom related to the oxygen atom, due to the position of the independent molecule on the mirror. In order to highlight this disorder, the hydrogen atoms whose occupancy rate is 0.5 are represented by full green and pink circles.

The cohesion of the structure is ensured both by hydrogen bonds and van der Waals interactions alternatively (see Figure 2-a and 2-b). Figure 2-e shows the arrangement of the hydrogen bonds in phase I at 275K. The structure consists on a 3D hydrogen bond network within the *along b* plane but connecting molecules along the b axis (see Figure 2-a) in such a way that 6 molecules form an hexagon shaped structure (Figure 2-e) in which molecular dipoles point to. The intermolecular distances O···O of hydrogen bond are between 2.628 Å and 2.644 Å, and the angles O-H···O range from 154° to 158° for the two independent molecules (see Table 1). These results reflect strong hydrogen bonds and consistently, strong intermolecular interactions. The existence of a mirror implies that the hydrogen bond related to oxygen is disordered and then, the hydrogen atoms attached to the oxygen atom have an occupancy factor of 0.5. Such strong interactions are consisting with the high value of the melting entropy change, (6.34 ± 0.13)R, i.e., much higher than the characteristic value of 2.5R established by Timmermans [51] as an upper bound for orientationally disordered (plastic) phases. On these grounds, 1-adamantane-methanol is one of the few 1-X-adamantane derivatives without a high-temperature orientationally disordered phase.

On cooling from phase I to phase II, single crystal was always damaged, so the structure of phase II was undertaken through high-resolution X-ray powder diffraction. The lattice of the low-temperature phase II was determined at 90 K as monoclinic by means of X-Cell software, available in the module Powder Indexing of Materials Studio. Systematic absences enable us to determine the space group, which was compatible with $P2_1/n$ space group and according to a reasonable density and compatibility between the zero volume change at the II-I transition, Z=12 was assigned. Pawley refinement [52], which minimizes the weighted R-factor, R_{wp}, describing the agreement between the experimental and the simulated patterns, helps to confirm the indexing result and the systematic absences, thus confirming the space group. The unit-cell parameters refined are gathered in Table 2. The final Rietveld refinement [53], position and orientation of the molecule, within the rigid-body constraint, with a single overall isotropic displacement parameter and preferred orientation were refined using the Rietveld-Toraya function [54]. The final refined pattern is depicted in Figure 3 together with the experimental and refined pattern difference. The representation of the structure obtained for phase II is displayed in Figure 2-d (in this figure the hydrogen atoms are represented by full pink circles). Broadly speaking, the overall packing of phase II is quite similar to that of phase I, with the obvious difference of the breakdown of the mirror plane. The arrangement of the hydrogen bonds for phase II at 90K are presented in Figure 2-f. The shorter O···O hydrogen bonds distances in phase II are 2.587Å and 2.604Å, with O-H···O angles of 172° and 171°, close but shorter than those present in phase I, indicating a slightly stronger intermolecular interactions.

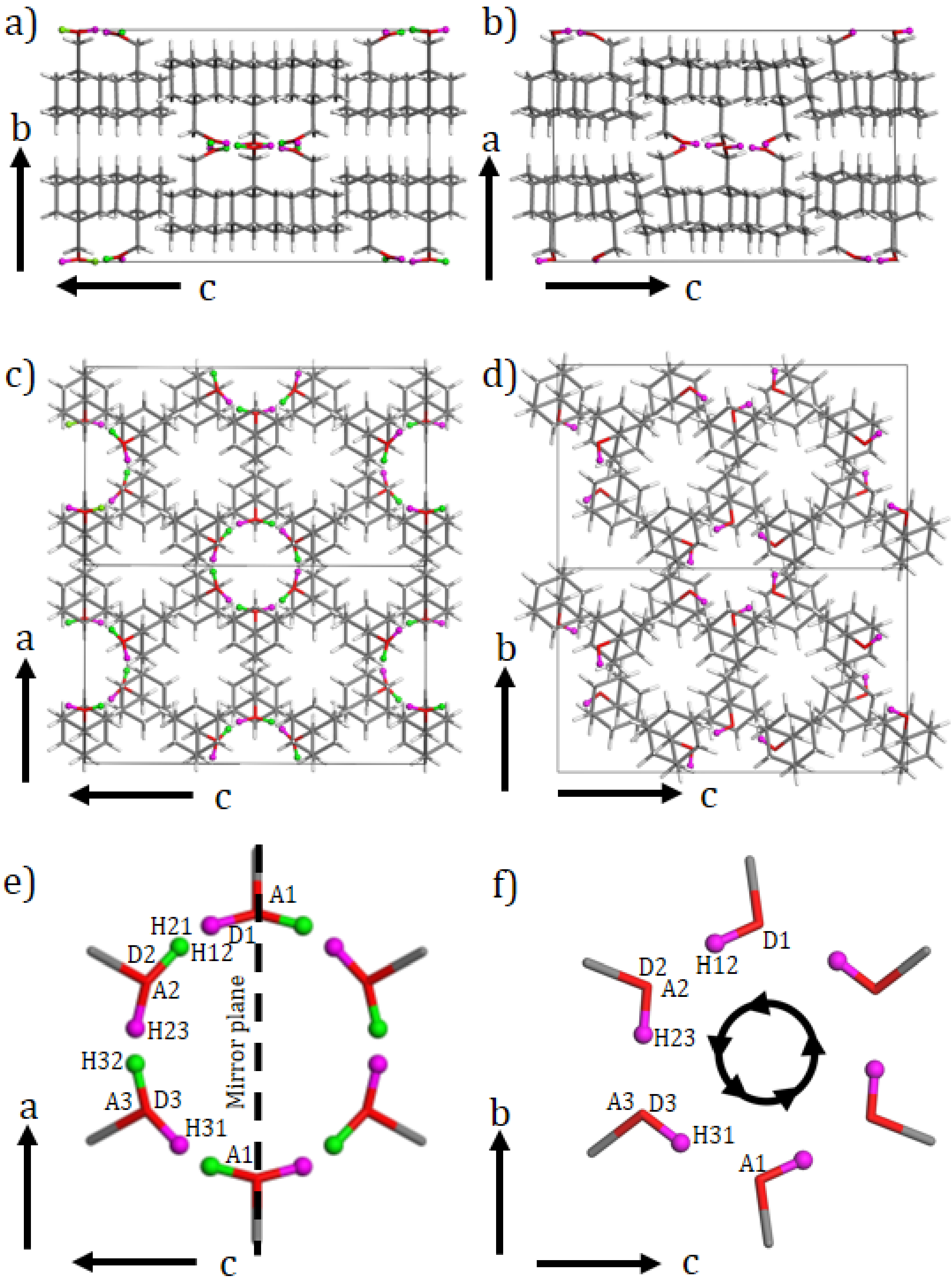

Figure 2: Crystal structures of 1-adamantane-methanol phase I at 275 K (left panels, (a) *along a* and (c) *along b*) and phase II at 90 K (right panels, (b) *along b* and (d) *along a*). Figures (e) and (f) depict the intermolecular hydrogen bond scheme for phases I (*along b* planes) and II (*along a* planes), respectively. *A* and *D* indicate the acceptor and donor character of the oxygen atoms.

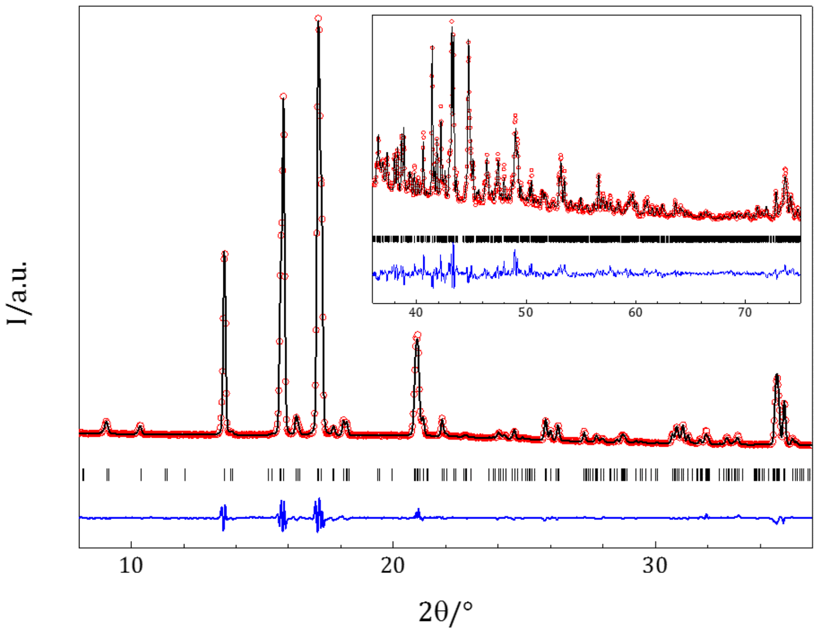

Figure 3: Experimental (red circles) and Rietveld refined (black line) diffraction patterns along with the difference profile (blue line) and Bragg reflections (vertical sticks) of the monoclinic $P2_1/n$ space group phase II of 1-adamantane-methanol at 90 K. Insert corresponds to the scale for the data between 35° and 75° magnified 10 times.

Table 1: The hydrogen bond angles (O-H···O) and distances (O···O) for phases I and II.

Phase	**Angles O-H···O**	**(°)**	**Distances O···O**	**(Å)**
I	D1-H12···A2	154	D1···A2	2.628
	D2-H21···A1	157	D2···A1	2.628
	D3-H32···A2	158	D3···A2	2.644
II	D1-H12···A2	172	D1···A2	2.587
	D2-H23···A3	171	D2···A3	2.604
	D3-H31···A1	168	D3···A1	2.725

In order to check the intermolecular interactions, the isobaric thermal-expansion tensor has been determined. [55-57]

To do so, lattice parameters as a function of temperature from 90 K to 360 K were measured (see Table S1). Patterns were collected every 30 K and every 5 K close to the II-I transition. The variation of the lattice parameters with temperature is shown in figures 4-a to 4-d. For the continuity in the settings, we present a_{II} with b_I and b_{II} with a_I. The continuity in the variation of the parameters and the volume (see Figure 4) as a function of temperature ascertain that the phase change is provided by a second-order transition with virtually no volume change, as revealed by the thermodynamic measurements.

Table 2: Crystal data for phases I and II of 1-adamantane-methanol from the X-ray single crystal and powder diffraction analyses, respectively.

Structure	**Phase II**	**Phase I**
Formula	$C_{11}H_{18}O$	$C_{11}H_{18}O$
FW(g.mol^{-1})	166.25	166.25
Crystal system	monoclinic	orthorhombic
Space group	$P2_1/n$	Pnnm
T(K)	90(2)	275(2)
Wavelength (Å)	1.5406	1.54187
Unit cell dimensions (Å)	a= 13.0675(7)	a= 11.4489(8)
	b= 11.2831(8)	b= 13.1094(9)
	c= 19.3721(14)	c= 19.6876(14)
	α= 90°	α= 90°
	β= 90.518°(5)	β= 90°
	γ= 90°	γ= 90°
Z(Z')	12(3)	12(1.5)
V(Å^3)	2856.1(3)	2954.9(4)
D_x(g.cm^{-3})	1.160	1.121
R_{wp}	4.69 %	
R_p	3.32 %	
R_1, (I>2σ(I))		6.9 %
wR_2, (I>2σ(I))		16.75 %
R_1		10.65%
wR_2		18.15%

The lattice parameters and unit cell volume were fitted by a standard least-squares method as a function of temperature, and the polynomials describing such a temperature variation are compiled in Table S2.

The thermal-expansion tensors are represented in figure 5 for three temperatures. For the monoclinic phase, the tensor is defined by the principal coefficients, α_1, α_2 and α_3 and an angle between the principal direction and the crystallographic 2-fold axis ***b***, while for the orthorhombic phase, the eigenvectors are being coincident with the crystal axes. Figure 5d shows the variations of the eigenvalues as a function of temperature for the two phases. Although the hydrogen bonds are mainly in the (bc) plane, the thermal expansion reveals stronger interactions in the direction α_1 (the "hard" direction) close to ***a***, in which even negative values (contraction) are found. The soft direction, i.e., that with the weakest interaction (α_3) lies within the (00l) plane. Such a direction for phase II becomes softer when approaching the II to I transition, due to the oncoming appearance of the mirror plane.

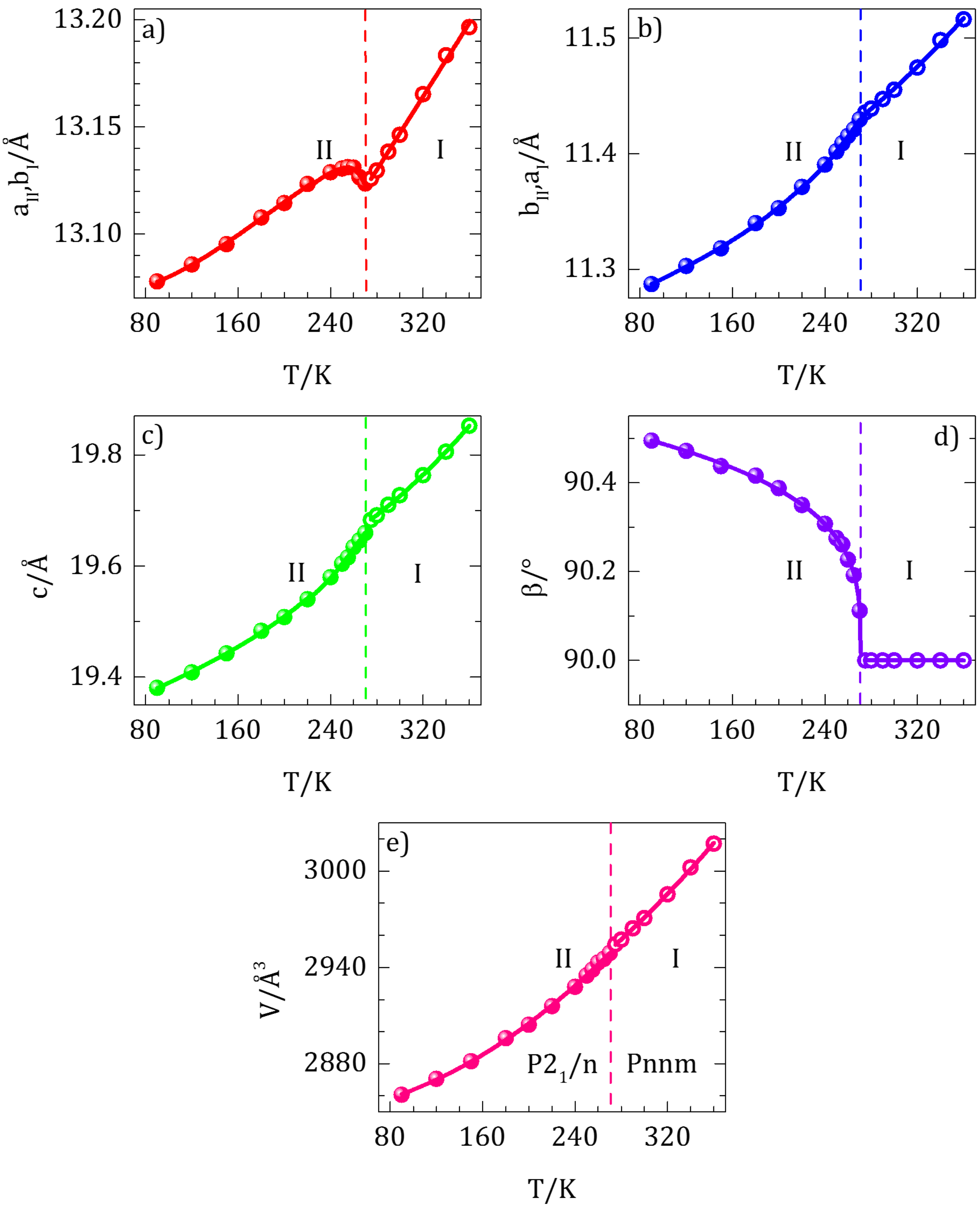

Figure 4: Variation of the lattice parameters and the volume as a function of temperature for phases II (full circles) and phase I (empty circles). Lines are the polynomial fits (see Table S2 in supplementary Information). The error bars are smaller than the size of the points.

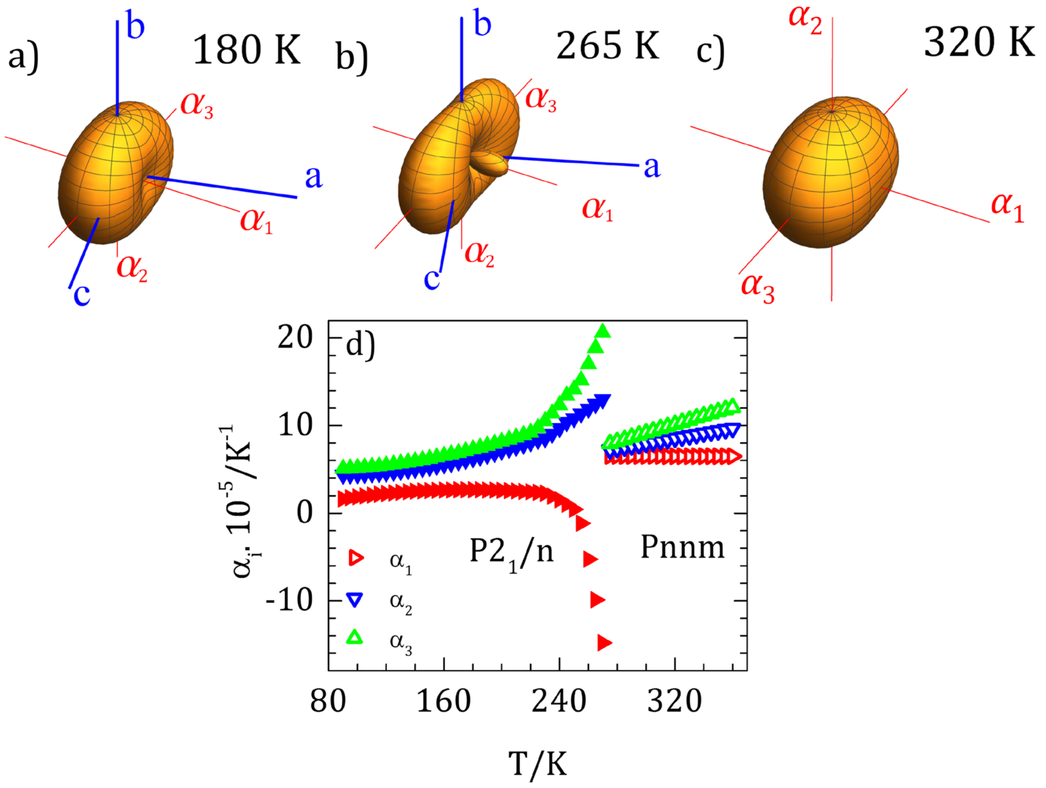

Figure 5: Thermal-expansion tensors for P2$_1$/n monoclinic phase II (a and b) and Pnnm orthorhombic phase I (c) and the eigenvalues α_i for the orthorhombic (empty symbols) and monoclinic (full symbols) phases as a function of temperature (d).

According to the temperature variation of the β parameter (see Figure 4-d) in which the β angle changes continuously on cooling from 90^o around T$_c$ to higher values and the subgroup-group relation between phase I and phase II, an order parameter η for a continuous (second order) II to I transition can be defined as:

$$\eta(T)=\eta_0+\left(\beta(T=0)-90^o\right)\left[1-\frac{T}{T_c}\right]^{\gamma} \tag{1}$$

where $\eta_0=90^o$ is the orthorhombic angle of phase I, $\beta(T=0)$ is the β angle at T=0 K, T_c is the critical transition temperature and γ is the critical exponent. A fit of eq.(1) to the phase II data gives rise to T_c=270.71±0.18K, close to the calorimetric phase transition, and γ=0.269±0.004, close to the theoretical prediction of 3D microscopic Ising model.i.e. 0.33. [58]

This order-disorder phase transition can be interpreted microscopically by means of the disorder of the H atom linked to the O atom, lying on the mirror, in phase II, as it is for phase I, in which the H atom displays an occupancy factor of 50% (in both sides of the mirror plane, Figure 2-e). Thus, on cooling phase II the H atom would increase the difference of the occupational factor between the two sites, as described in Figure 2-f. In fact, at 90 K, the lowest temperature at which the structure has been solved, the occupancy factor of one of the sites (pink atom) is close to 1, with values of the angles of the hydrogen bonds close to 180° (the arrows in figure 2-f indicate the direction of the most probable direction of Donor, Acceptor directions). Within this image the decrease of the order parameter on increasing temperature (Figure 6) would be accompanied with an increase of the "*symmetrization*" of the occupational factor of the H atom of the hydroxyl group up to equal values (50%) at $T=T_c$, the temperature at which the equality of the occupational factors (together with the value of $\beta=90^o$) makes the appearance of the symmetry plane and thus, leading to the lattice the Pnnm symmetry. Second-order phase transitions involving organic hydrogen-bonded crystals have recently been described [59-61] and even a Landau theory using an expansion of the free energy has been proposed [62-63].

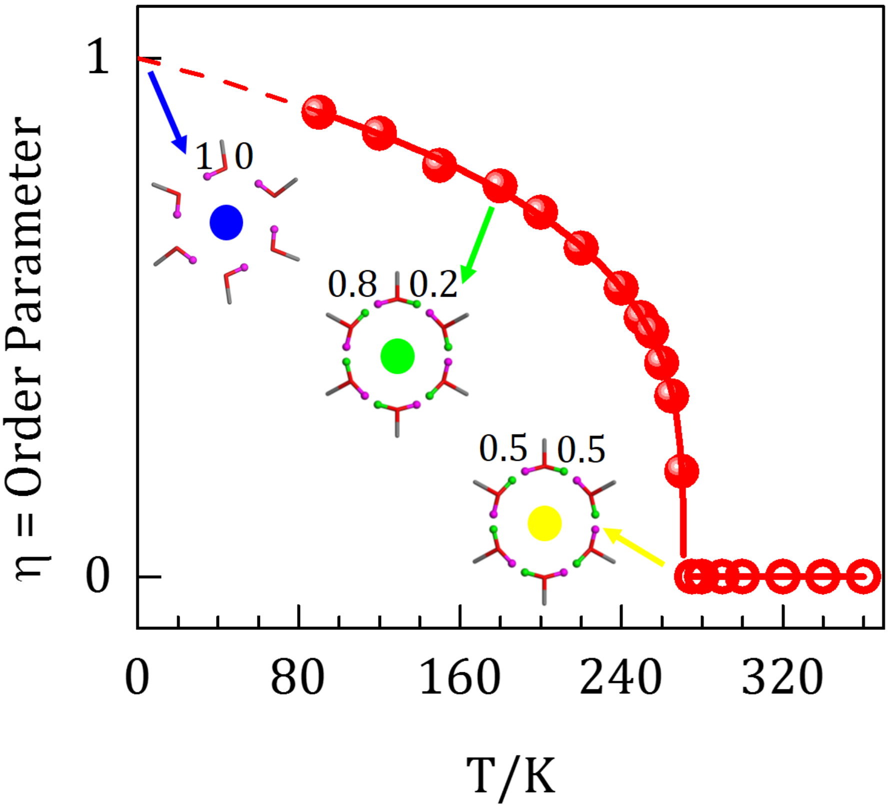

Figure 6: Order parameter η as a function of temperature for monoclinic phase I (full circles) and orthorhombic phase II (empty circles). Line corresponds to the fit according to equation (1). Pictures along the order parameter curve are hydrogen bond schemes with the occupational factor for the hydrogen of the -OH group.

4. Conclusion

The polymorphism of 1-adamantane-methanol has been studied from 90K to the liquid state. The low-temperature phase II, which was found to be monoclinic with space group $P2_1/n$ (Z=12, Z'=3) transforms to the high-temperature phase I with space group Pnnm (Z=12, Z'=1.5). The passage from the monoclinic phase to the orthorhombic phase is conducted by means of a second-order phase transition which carries a group-subgroup relationship, and its order is proved by a continuous tilt of the c-axis. The resolution of the crystal structures of both phases was carried out by exploiting X-ray diffraction data on powder (phase II) and on single-crystal (phase I). Both structures have a very close stacking of molecules with strong hydrogen bonds. Although both phases are built up through a 12 molecules per unit lattice, the number of independent molecules is reduced through a second order phase transition which breaks the mirror symmetry present in phase I. The pressure-temperature phase diagram does not reveal the appearance of new phases. The volume and entropy change at the melting as well as the slope $\left(\frac{dT}{dp}\right)_{I\to L}$ of the two-phase coexistence curve thermodynamically reinforce the disordered character of phase I highlighted by the structural study, unlike most of 1-X-adamantane derivatives.

ASSOCIATED CONTENT

■ Supporting Information

Crystallographic information files (CIF) for monoclinic and orthorhombic phases I (at 275 K) and II (at 90 K) of 1-Adamantane-methanol, lattice parameters as a function of temperature for both phases as well as their polynomial fits, and the melting and transition differential thermal analysis curves as a function of pressure. This material is available free of charge via the Internet at http://pubs.acs.org.

■ AUTHOR INFORMATION

Corresponding Author

*E-mail: josep.lluis.tamarit@upc.edu.

Notes

The authors declare no competing financial interest.

Acknowledgements

This work has been partially supported by the Spanish Ministry of Science and Innovation through project FIS2014-54734-P and by the Generalitat de Catalunya under project 2014 SGR-581.

References

(1) Wang, Y.Y.; Kiopakis, E.; Lu, X.H.; Wegner, D.; Yamachika, R.; Dahl, J. E.; Carlson, R. M. K.; Louie, S. G.; Crommie, M. F. *Nature Mater.* **2008**, *7*, 38-42.

(2) Yang, W. L.; Fabbri, J. D.; Willey, T. M.; Lee, J. R. I.; Dahl, J. E.; Carlson, R. M. K.; Schreiner, P. R.; Fokin, A. A.; Tkachenko, B. A.; Fokina, N. A.; Meevasana,W.; Mannella, N.; Tanaka, K.; Zhou, X. J.; van Buuren, T.; Kelly, M. A.; Hussain, Z.; Melosh, N. A.; Shen, Z.-X. *Science* **2007**, *316*, 1460-1462.

(3) Du, Q. -S.; Huang, R. -B. *CurrentProtein and Peptide Science* **2012**, *13*, 205-210.

(4) De Clercq, E. *J. Clin. Virol.* **2004**, *30*, 115-133.

(5) Nicholson, K. G.; Wood, J. M.; Zambon, M. *Lancet* **2003**, *362*, 1733-1745.

(6) Cheon, Y.E.; Suh, M. P. *Chem.-Eur. J.* **2008**, *14*, 3961-3967.

(7) Elsaidi, S. K.; Mohamed, M. H.; Wojtas, L.; Chanthapally, A.; Pham, T.; Space, B.; Vittal, J. J.; Zaworotko, M. J. *J. Am. Chem. Soc.* **2014**, *136*, 5072-5077.

(8) Schoedel, A.; Zaworotko, M. *J. Chem. Sci.* **2014**, *5*, 1269-1282.

(9) Yamamoto, A.; Uehara, S.; Hamada, T.; et al. *Cryst. Growth Des*. **2012**, *12*, 4600-4606.

(10) Gunawan, M. A.; Hierso, J.-C.; Poinsot, D.; et al. *N. J. Chem.* **2014**, *38*, 28-41.

(11) Hohman, J. N.; Claridge, Sh. A; Kim, M.; Weiss, P.S. *Mater. Sci. Eng. R* **2010**, *70,* 188-208.

(12) McIntosh, G. C.; Yoon, M.; Berber, S.; Tomanek, D. *Phys. Rev. B* **2004**, *70*, 045401.

(13) Vijayakumar, V.; Garg, A. B.; Godwal, B. K.; Sikka, S. K. *Chem. Phys. Lett*. **2000**, *330*, 275-280.

(14) Zhang, M.; Zukoski, Ch. F. *Langmuir* **2014**, *30*, 7540-7546.

(15) Negrier, Ph.; Barrio, M.; Tamarit, J. Ll.; Mondieig, D. *J. Phys. Chem. B* **2014**, *118*, 9595-9603.

(16) Bazyleva, A. B.; Blokhin, A. V.; Kabo, G. J.; Kabo, A. G.; Sevruk, V. M. *Thermochim. Acta.* **2006**, *451*, 65-72.

(17) Romanini, M.; Negrier, P.; Tamarit, J. Ll.; Capaccioli, S.; Barrio, M.; Pardo, L. C.; Mondieig, D. *Phys. Rev. B* **2012**, *85*, 134201.

(18) Harvey, P. D.; Butler, I. S.; Gilson, D. F. R.; Wong, P. T. T. *J. Phys. Chem.* **1986**, *90*, 4546-4549.

(19) Negrier, P.; Barrio, M.; Romanini, M.; Tamarit, J. Ll.; Mondieig, D.; Krivchikov, A. I.; Kepinski, L.; Jezowski, A.; Szewczyk, D. *Cryst. Growth Des.* **2014**, *14*, 2626-2632.

(20) Hara, K.; Katou, Y.; Osugi, J. *Bull. Chem. Soc. Jpn*. **1981**, *54*, 687-691.

(21) Paroli, R. M.; Kawaii, A. T.; Butler, A. S.; Gilson, D. R. *Can. J. Chem.* **1988**, *66*, 1973-1978.

(22) Hara, K.; Taniguchi, J.; Suzuki, K. *Chem. Lett.* **1980,** *7*, 803-806.

(23) Clark, T.; Mckervey, M. A.; Mackle, H.; Rooney, J. J. *Chem. Soc. Faraday. Trans.* **1974**, *70*, 1279-1291.

(24) Foulon, M.; Grors, C. *Acta. Cryst. Sect. B* **1988**, *44*, 156-163.

(25) Foulon, M.; Amoureux, J. P.; Sauvajol, J. L.; Lefebvre, J.; Descamps, M. *J. Phys. C.* **1983**, *16*, L265-L269.

(26) Martinez-Garcia, J. C.; Tamarit, J. Ll.; Capaccioli, S.; Barrio, M.; Veglio, N.; Pardo, L. C. *J. Chem. Phys.* **2010**, *132*, 164516.

(27) Clark, T.; Knox, T. M. O.; Mackle, H.; Mckervey, M. A. *J. Chem. Soc. Faraday. Trans.* **1977**, *73*, 1224-1231.

(28) Virlet, J.; Quiroga, L.; Boucher, B.; Amoureux J. P.; Castelain, M. *Mol. Phys.* **1983**, *48*, 1289-1303.

(29) Braga, D.; Koetzle, T. F. *Acta Cryst. B* **1988**, *44*, 156-163.

(30) Decressain, R.; Amoureux, J. P.; Carpentier, L.; Nagy, J. B. *Mol. Phys.* **1991**, *73*, 553-569.

(31) Foulon, M.; Belgrand, T.; Gors, C.; More, M. *Acta Cryst. B* **1989**, *45*, 404-411.

(32) Affouard, F.; Hedoux, A.; Guinet, Y.; Denicourt, T.; Descamps, M. *J. Phys.: Condens. Matter* **2001**, *13*, 7237-7248.

(33) Amoureux, J. P.; Sauvajol, J. L.; Bee, M. *Acta Cryst. A* **1981**, *37*, 97-104.

(34) Amoureux, J. P.; Bee, M.; Sauvajol, J. L. *Acta Cryst. B* **1982,** *38*, 1984-1989.

(35) Bee, M.; Amoureux, J. P. *Mol. Phys.* **1983**, *48*, 63-79.

(36) Betz, R.; Klüfers, P.; Mayer, P. *Acta Cryst. E* **2009**, *65*, o101.

(37) Manosa, Ll.; Gonzalez-Alonso, D.; Planes, A.; Bonnot, E.; Barrio, M.; Tamarit, J. Ll.; Aksoy, S.; Acet, M. *Nature Mater.* **2010**, *9*, 478-481.

(38) Ballon, J.; Comparat, V.; Pouxe, J. *Nucl. Instrum. Methods* **1983**, *217*, 213-216.

(39) Evain, M.; Deniard, P.; Jouanneaux, A.; Brec, R. *J. Appl. Crystallogr.* **1993**, *26*, 563-569.

(40) MS Modeling (Materials Studio), version 5.5: http://www.accelrys.com.

(41) Rigaku. *Crystalclear-sm expert 2.1. Software*, **2013**.

(42) Sheldrick, G. M. *Acta Cryst. A* **2008**, *64*, 112-122.

(43) Farrugia, L. J. *J. Appl. Cryst.* **1999**, *32*, 837-838.

(44) Andersson, S. P.; Anderson, O. *Macromolecules* **1998**, *31,* 2999-3006.

(45) Barrio, M.; Maccaroni, E.; Rietlveld, I. B.; Malpezzi, L.; Masciocchi, N.; Céolin, R.; Tamarit, J. Ll. *J. Pharm. Sci.* **2012**, *101*, 1073-1078.

(46) Negrier, P.; Barrio, M.; Tamarit, J. Ll. ; Mondieig D. *J. Phys. Chem. B* **2014**, *118*, 9595-9603.

(47) Negrier, P.; Barrio, M.; Romanini, M.; Tamarit, J. Ll.; Mondieig, D.; Krivchikov, A. I.; Kepinski, L.; Jezowski, A.; Szewczyk, D. *Cryst. Growth Des.* **2014**, *14*, 2626-2632.

(48) Hara, K.; Katou, Y.; Osugi, J. *Chem. Soc. Jpn.* **1981**, *54*, 687-691.

(49) Tamarit, J. Ll.; Rietveld, I. B.; Barrio, M.; Ceolin, R. *J. Mol. Struct.* **2014**, *1078*, 3-9.

(50) Reuter, J.; Busing, D.; Tamarit, J. Ll.; Wurflinger, A. *J. Mater. Chem.* **1997**, *7*, 41-46.

(51) Timmermans, J. *J. Phys. Chem. Solids* **1961**, *18*, 1-8.

(52) Pawley, G. S. *J. Appl. Crystallogr.* **1981,** *14*, 357-361.

(53) Rietveld, H. M. *J. Appl. Crystallogr.* **1969**, *2*, 65-71.

(54) Toraya, H.; Marumo, F. *Mineral. J.* **1981**, *10*, 211-221.

(55) Salud J.; Barrio, M.; Lopez, D. O.; Tamarit, J. Ll.; Alcobé, X. *J. Appl. Crystallogr.* **1998**, *31*, 748-757.

(56) Tamarit, J. Ll.; Lopez, D. O.; Alcobé, X.; Barrio, M.; Salud, J.; Pardo, L. C. *Chem. Mater.* **2000**, *12,* 555-563.

(57) Negrier, P.; Pardo, L. C.; Salud, J.; Tamarit, J. Ll.; Barrio, M.; Lopez, D. O.; Würflinger, A.; Mondieig, D. *Chem. Mater.* **2002**, *14,* 1921-1929.

(58) Pelissetto, A.; Vicari, E. *Phys. Rep.* **2002**, *368*, 549-727.

(59) Chantrapromma, S.; Fun, H. -K.; Usman, A. *J. Mol. Struct.* **2006**, *789*, 30-36.

(60) Ye, H. -Y.; Ge, J. -Z.; Chen, F.; Xiong, R. -G. *CrystEngComm.* **2010**, *12*, 1705-1708.

(61) How, P. T.; Lee, B. S.; Fun, H. -K.; Razak, I. A.; Chantrapromma, S. *Phys. Rev. B* **2005**, *71*, 174109.

(62) Fun, H.-K.; Usman, A.; Chantrapromma, S.; Osman, J.; Ong, L. -H.; Tilley, D. R.; Ishibashi, Y. *Solid State Commu.* **2003**, *127*, 677-682.

(63) Rosli, M. M.; Lee, B. S.; Fun, H. -K. *Phys. Status Solidi B* **2009**, *246*, 376-382.

For Table of Contents Use Only

Phase transition in hydrogen-bonded 1-adamantane-methanol

Bacem Ben Hassine, Philippe Negrier, María Barrio, Denise Mondieig,
Stéphane Massip and Josep Ll. Tamarit

TOC graphic

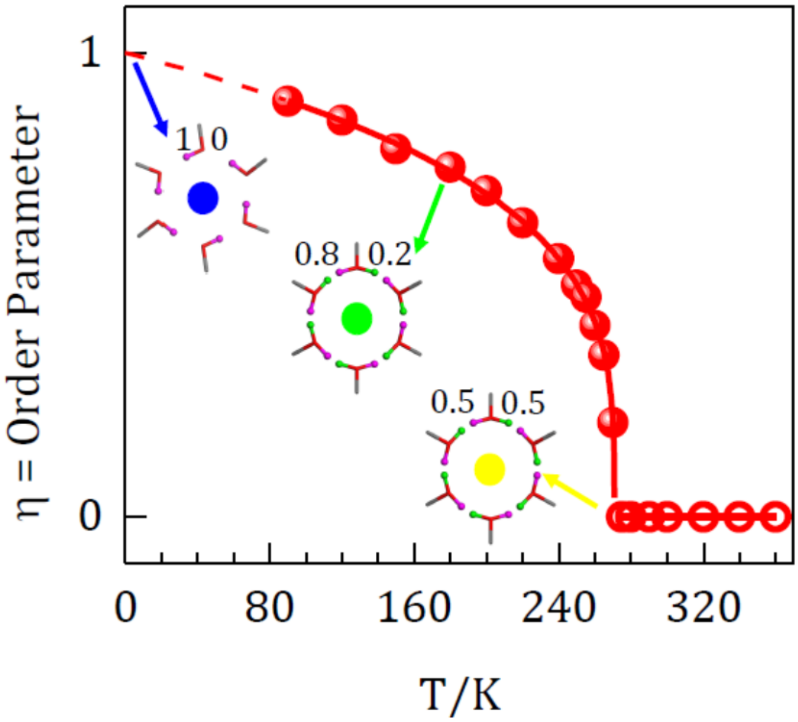

Synopsis

1-adamantane-methanol ($C_{11}H_{18}O$) exhibits a low-temperature monoclinic ($P2_1/n$, Z=12, Z'=3) phase which transforms at 272 K to an orthorhombic (Pnnm, Z=12, Z'=1.5) phase through a continuous order-disorder phase transition which carries a group-subgroup relationship, and its order is proved by a continuous tilt of the monoclinic c-axis.